Nanoscale

Structural Evolution of Two-Dimensional Silicates Using a "Bond-Switching" Algorithm

Journal:	*Nanoscale*
Manuscript ID	NR-ART-10-2020-007623.R1
Article Type:	Paper
Date Submitted by the Author:	19-Nov-2020
Complete List of Authors:	Boscoboinik, Jorge; Brookhaven National Laboratory, Center for Functional Nanomaterials Manzi, Sergio; Universidad Nacional de San Luis, Departamento de Física, Instituto de Física Aplicada (INFAP) - CONICET Pereyra, Victor; Universidad Nacional de San Luis, Departamento de Física, Instituto de Matemática Aplicada (IMASL) - CONICET Boscoboinik, Alejandro; University of Wisconsin-Milwaukee, Department of Chemistry and Biochemistry and Laboratory for Surface Studies Mas, Walter; Universidad Nacional de San Luis, Departamento de Matemática

Structural Evolution of Two-Dimensional Silicates Using a "Bond-Switching" Algorithm

Alejandro M. Boscoboinik[1], Sergio J. Manzi[2,*], Víctor D. Pereyra[3], Walter L. Mas[4], Jorge Anibal Boscoboinik[5,*]

[1] Department of Chemistry and Biochemistry and Laboratory for Surface Studies, University of Wisconsin–Milwaukee, Milwaukee, Wisconsin 53211, United States.
[2] Departamento de Física, Instituto de Física Aplicada (INFAP) - CONICET, Universidad Nacional de San Luis, Chacabuco 917, San Luis 5700, Argentina.
[3] Departamento de Física, Instituto de Matemática Aplicada (IMASL) - CONICET, Universidad Nacional de San Luis, Chacabuco 917, San Luis 5700, Argentina
[4] Departamento de Matemática, Universidad Nacional de San Luis, Ejército de los Andes 950, San Luis 5700, Argentina.
[5] Center for Functional Nanomaterials, Brookhaven National Laboratory, Upton, New York 11973-5000, United States.

Corresponding authors: smanzi@unsl.edu.ar, jboscoboinik@bnl.gov

Abstract

Silicates are the most abundant materials in the earth's crust. In recent years, two-dimensional (2D) versions of them grown on metal supports (known as bilayer silicates) have allowed their study in detail down to the atomic scale. These structures are self-containing. They are not covalently bound to the metal support but interact with it through Van der Waals forces. Like their three-dimensional counterparts, the 2D-silicates can form both crystalline and vitreous structures. Furthermore, the interconversion between vitreous to crystalline structures has been experimentally observed at the nanoscale. While theoretical work has been carried out to try to understand these transformations, a limitation for ab-initio methods, and even molecular dynamics methods, is the computational cost of studying large systems and long timescales. In this work, we present a simple and computationally inexpensive approach, that can be used to represent the evolution of bilayer silicates using a bond-switching algorithm. This approach allows reaching equilibrium ring size distributions as a function of a parameter that can be related to the ratio between temperature and the energy required for the bond-switching event. The ring size distributions are compared to experimental data available in the literature.

1. Introduction

Silicates are the most abundant materials in the earth's crust. While diffraction methods have allowed resolving crystalline structures in detail, vitreous structures have been relegated due to the lack of experimental methods that allow their detailed study at the atomic scale. However, vitreous structures are crucial in diverse applications (e.g. electronic devices, optic fibers, solar cells, catalysts, etc.) and exhibit issues of fundamental interest that are difficult to understand due its structural complexity. In 2012, the first atomically resolved images of a two-dimensional silicate glass were reported almost simultaneously and independently by two groups using scanning tunneling microscopy (STM)[1] and transmission electron microscopy (TEM).[2] These works constitute the materialization of a well-known theoretical model proposed 80 years earlier by Zachariasen.[3] These experimental model systems opened the possibility of exploring in detail the structure of silicate glasses, especially in combination with theoretical and simulation methods. [4] Note that the imaging methods mentioned above used to determine the presence of vitreous structures (STM and TEM) are not sufficient to determine the bilayer nature of these silicates. It was prior work by Loffler et al [5], using infrared reflection absorption spectroscopy, that allowed the identification of the bilayer nature of these silicates as evidenced by a strong phonon vibration at 1300 cm^{-1}, later also found in the vitreous forms.

While in a crystal it is sufficient to know a unit cell to describe a system completely, in a glass it is necessary to consider large regions so that the description is representative of the system under study. It is then that low cost computational methods such as Monte Carlo simulations using lattice gas models[6] become suitable for studying this type of systems, in contrast to ordered systems for which calculations based on quantum mechanics are typically carried out. The bilayer silicates that were reported and well characterized experimentally can be obtained in their vitreous (glassy)[1] or crystalline forms, where the crystalline form is manifested by a distinctive (2×2) structure in its low energy electron diffraction (LEED) pattern [5], while the vitreous one is characterized by a ring going through where the (2×2) spots would be. However, there does not seem to be a reliable way to predict which phase will be obtained. Seemingly identical conditions give sometimes crystalline and some other times vitreous structures. Suggestions related to the cooling rate and other parameters influencing the resulting structure have been made and this is matter of active debate. Useful information that can aid in the understanding of this process has been recently reported by Klemm et al [7], [8] where initial, intermediates and transition structures for the formation of a Stone-Wales defect are proposed via ab initio calculations. In that work, LEED I-V analysis was also shown to be feasible to obtain structural information including the bilayer nature of the silicate structure as well as the support. From the experimental experience of one of us (JAB) working on the synthesis of these 2D-materials, in some cases there is no conclusive evidence to determine the crystallinity of the structure with certainty *a priori*. This is a fascinating observation from a fundamental point of

view of the crystallization process, but also of great importance in applications since the electronic and adsorptive properties depend on the crystallinity of the material. In fact, silicates having both glassy and crystalline domains on the same sample have been obtained.[9] In relation to this, another important detail is the influence of the support where the structure is formed. For the case in which both vitreous and crystalline regions can be obtained, the structures were produced on the face (0001) of a Ruthenium crystal. However, when Pt(111) is used, which has a lattice constant larger than Ru(0001), only vitreous structures [10] are obtained. Pd(111) and Pd(100) crystals tend to give crystalline bilayer SiO_2 structures. When more oxophilic metals are used, Si-O-metal linkages are formed preventing the formation of bilayer structures.[11]

Side and top views of the structural model of these 2D-silicates (crystalline version) are shown in Figures 1a and 1b, respectively. These structures are composed a 2D-arrangement of polygonal prisms (hexagonal prisms in the crystalline case) in which the corners of the prism are occupied by Si atoms while the edges are the O linkages between adjacent Si atoms. To simplify, we will use a wireframe representation of these materials in the rest of the manuscript, showing only the top view. Figure 1c shows such wireframe representation of the model in Figure 1b, where the edges of the prisms (Si-O-Si linkages) are represented as straight lines.

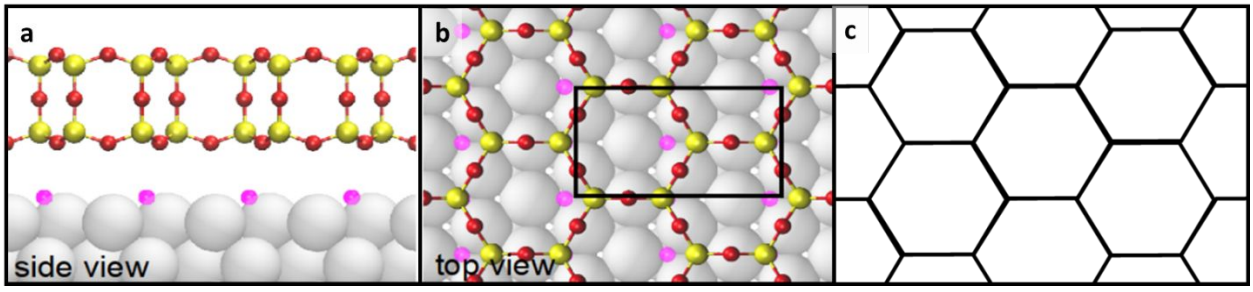

Figure 1. Side view (a) and top view (b) of crystalline bilayer silica structure on a metal support. A wireframe representation of the top view is shown in panel c, where the vertices of the hexagons represent the location of Si atoms, and the lines represent the O bridges.

Note that while we have described this structure as a 2D-array of polygonal prisms, it can also be seen as two identical layers linked by O-bridges (thus the commonly used name “bilayer”). Each silicon atom is bound to four oxygen atoms, three in the plane, and one between the two layers. It is important to note that there is a plane of symmetry in the middle of the two layers (they are mirror images), even for the vitreous structure. This means that, although it is vitreous in two dimensions, the structure is symmetric in the direction normal to the surface plane (if the metal support is ignored). Figure 2 shows TEM and corresponding structural models for crystalline and vitreous regions (adapted with permission from reference [2], Copyright (2020) American Chemical Society).

Since the two layers of this structure are mirror images, the description of one of the layers is sufficient to describe the system. In fact, the experimental methods to visualize the structure in

direct space, STM and TEM, only give information on one of the layers. The presence of a second layer was determined through the observation of phonon vibrations in the infrared region, associated with the oxygen linkage between the two layers.[11]

In addition to studying these materials to improve our fundamental understanding, the detailed knowledge of these structures is of great importance in catalysis, since the silicates are used as support materials for metal particles and may even have a great influence on the activity of the catalyst, due to the interaction between the silicate and the particles. A specific example is the Phillips catalyst, which consists of Chromium supported in SiO_2 matrix, promoting the polymerization of ethylene to form the most used polymer (Polyethylene).[12] Other related materials of great importance are zeolites, which catalyze some of the most important reactions in the industry, such as crude oil cracking and the synthesis of fuels from methanol. In fact, model systems for zeolites, with the same bilayer structure as the silicates described here, have recently been synthesized by producing an Al-doped silicate bilayer.[13] A notable difference in vitreous regions between the cases of bilayer silica and bilayer aluminosilicates is the distribution of rings, such that in the latter, rings with even numbers of sides [14] are more favored relative to silica. This is related to the Lowenstein rule of zeolites,[15] which specifies that Al-O-Al bonds cannot be formed in these structures, resulting in rings with the presence of alternating Si and Al atoms in tetrahedral positions (Si-O-Al-O-Si), favoring an even number of sides.[14] Another area in which understanding the ring size distribution in bilayer silicates will be of great importance is that of chemistry in confinement[16] (which has been shown to take place between the silicate and its metal support)[17][18][19], since the permeability of molecules to access such interface will depend on the size of the polygonal prims they have to pass through.[20]

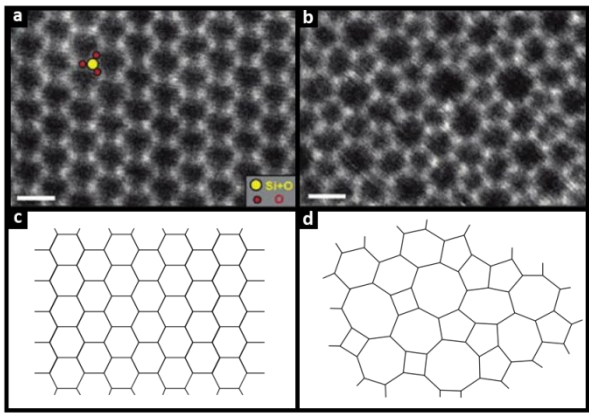

Figure 2. TEM images of a crystalline (a) and vitreous (b) regions with atomic resolution. Schematically, the models of the structures are shown in (c) and (d) respectively. Figure adapted from reference [2].

Considering the importance of these materials, the prediction of their ring size distribution can add critical value to their atomic-scale understanding. However, the use of ab-initio methods to calculate the energetics of vitreous silicates is prohibitively expensive. A possible alternative for such a problem is the use of simulation methods. Among the different options, we have chosen to use the Monte Carlo simulations and lattice gas models. These simulation methods have been widely used in statistical physics since its original version proposed in the 50s by Nicholas

Metropolis.[21] Over recent years numerous efforts have been made to improve the original algorithm, tending to analyze and understand systems in equilibrium and non-equilibrium.[22]

In terms of the generation of structural models for amorphous solids using Monte Carlo simulation, the most versatile model is the bond-switching with energy minimization (relaxation). One of the first works in which this algorithm is used was the one made by Wooten and Wearie [23], [24] for the generation of a model of amorphous silicon and germanium. This type of computer modeling has been extended in recent years to larger systems, including periodic boundary conditions, by Barkema and Mousseau [25]–[27] and by Vashishta and collaborators.[28]

The study of vitreous structures has a long history. The scheme of the structure of a glass proposed by Zachariasen in 1932, has been reproduced in countless opportunities.[3] The work related to simulations of glasses is extensive, and we are only going to briefly describe those related to the use of Monte Carlo methods for two-dimensional systems,[29] which are the most relevant to our work. A recent publication describes the case of amorphous graphene, which is generated experimentally by electron irradiation of graphene.[30] A similar structure is reproduced using Monte Carlo methods with the algorithm of "bond-switching".[31] This kind of algorithm has been applied to study the glass transition in self-organized cellular patterns by Aste and Sherrington.[32] The model considers a perfect hexagonal network composed of N cells, each cell "i" has six neighbors, and three cells share the same vertex. The energy related to the generation of a bond switching event in bilayer silica starting from four six-member rings to produce two five-member and two-seven member rings (effectively making a Stone-Wales defect) was first shown as a viable pathway for crystalline-to-glass transitions by the Sauer group based on *ab-initio* calculations. [1] Heuer et al later used a Yukawa-type force field to reproduce experimental structural data (ring size distributions) from bilayer silica films.[33]–[35]

In this paper, we describe a simple approach to simulate structural changes in two-dimensional silicates, using Monte Carlo methods and a bond-switching algorithm. The model is described in section 2. In section 3, we present and discuss the results obtained from using this model to follow the evolution of a network of rings representing those polygonal prisms found in two-dimensional bilayer silicates, and we compare them with experimental data. In section 4, we summarize these results and present our conclusions.

2. Model and Simulations

Let us consider a square lattice with periodic boundary conditions, as shown by dashed lines in Figure 3. We chose to use a square lattice as this can be easily represented by a matrix when we write the code. We construct a network of rings in this lattice by first placing an edge of the ring (Si-O-Si linkage) in the center of each cell. We will refer to these as **rotatable linkages (RL)**. For simplicity, we will start with a perfectly crystalline hexagonal network. In this case, all RL will be oriented at 45° with respect to the horizontal dashed lines (-45° is equivalent), and they are shown in Figure 3 as short thicker lines. We then connect each end of the RLs to their two closest cells in the square lattice. These connections represent **non-rotatable linkages (NL)** and are shown as longer thinner lines in Figure 3. This results in a wireframe model representing a perfect hexagonal lattice. Other initial configurations are also possible.

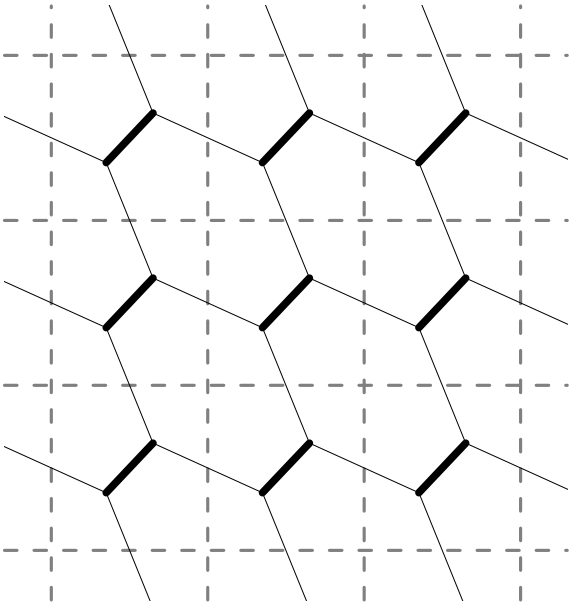

Figure 3. Hexagonal lattice formed in a square matrix, where the solid lines (sides of the hexagons) represent the Si-O-Si linkages in the silicate. The vertices in the hexagons correspond to Si atoms. Thick lines represent the rotatable Si-O-Si linkages (one per square cell) and the thin lines are non-rotatable linkages.

In this model, we will now allow RLs to rotate by 90°. An example of such rotation is shown in the shaded cell in Figure 4.

In this way, a 90° rotation of a given RL (see Figure 4) involves new assignments of its NLs. Each end of the RL are now linked to the two spatially closest ends of the RLs at the top, bottom, left, and right cells. The new NL assignment must preserve the number of NLs (two) at each end of the RL. In the example in Figure 4:

i) the upper end of the RL is now connected to the lower end of the RL in the upper cell and upper end of the RL in the left cell,

ii) the lower end is now connected with the upper end of the RL in the bottom cell and the lower end of the RL in the right cell.

As a result, when starting from a group of four 6-membered rings (6-6-6-6) a pair of 7- and a pair of 5-membered rings (5-5-7-7) are generated. This is commonly known as a Stone-Wales defect (SW) in a hexagonal lattice.

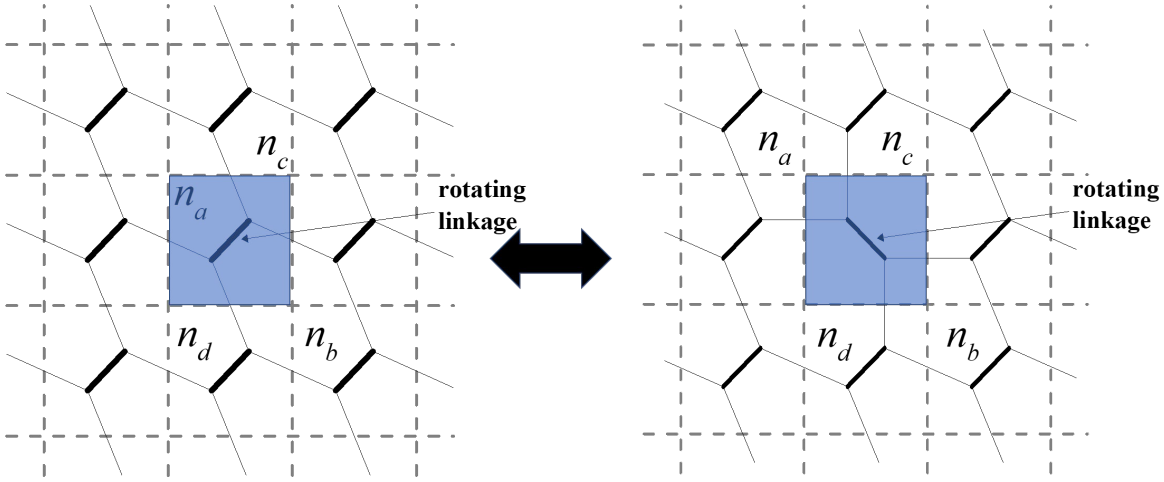

Figure 4. Representation of the rotation of a linkage by 90°, resulting in the conversion of four hexagons to two heptagons and two pentagons. Nearest and next-nearest neighbor cells corresponding to the rotating linkeage show the formation of a Stone-Wales defect (SW).

As a general rule when the RL of the cell under consideration is oriented at 45° (Figure 4a), its upper end is always connected to the RLs of the upper and right cells, while its lower end is always connected to the RLs of the lower and left cells. When the RL under consideration is oriented at -45° (Figure 4b) the upper end is connected to the RLs of the upper and left cells, and its lower end is connected to the RLs of the lower and right cells.

With this method (suggested by one of the authors W.L.M.), it is possible to obtain rings with different number of sides n, with $4 \leq n \leq 8$ (see Figure 5).

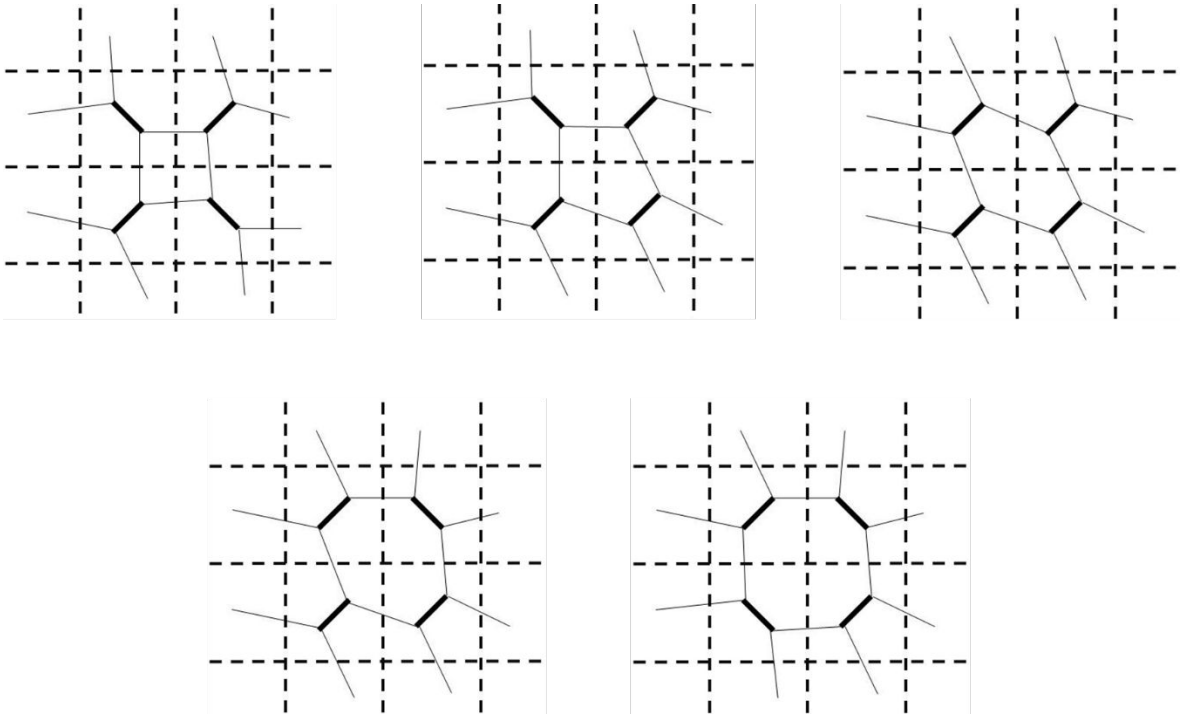

Figure 5: The five rings sizes that are possible to obtain with this algorithm are shown. There are 16 possible configurations: one for squares, four for pentagons, six for hexagons, four for heptagons and one for octagons.

Locally, the degree of deviation from the perfectly crystalline hexagonal structure can be measured in terms of the number of sides per cell. If n_i is the number of sides of ring i, then $q_i = 6 - n_i$ is a measure of its deviation from the hexagonal configuration.[32] Taking the crystalline configuration as a reference, we propose in this model that the increase of the energy of the system can be measured from its deviation from the crystalline structure using the following equation,

$$E = \varepsilon \sum_{i=1}^{N} q_i^2 = \varepsilon \sum_{i=1}^{N} (6 - n_i)^2 , \quad (1)$$

where, N is the total number of rings in the system and ε is a reference energy value.

The change of the energy associated with a linkage rotation is:

$$\Delta E(n_a,n_b;n_c,n_d) = 2\varepsilon(2 + n_c + n_d - n_a - n_b) , \quad (2)$$

where (n_c and n_d) n_a and n_b are scalars equal to the number of sides of the rings adjacent to the (next) nearest neighbors to the rotating linkage, see Figure 4 (e.g., $n_i = 6$ for a hexagon). After a rotation, the nearest neighbor rings become the next-nearest neighbor rings, and vice versa.

Kumar et al. [31] have used more elaborated physical potentials introduced by Keating [36] and Tersoff [37] to describe two-dimensional Zachariasen glasses by using the same methodology.

With a determined sequence of rotations, it is possible to find the different structures reported experimentally in the literature,[38] which are shown in Figure 6. The most common one is the Stone-Wales defect, but other shapes have been previously named as flower, butterfly, and tortoise. In our model these structures can be detected, and their formation sequence can be analyzed too. The equilibrium distribution of these structures as a function of temperature is shown in figure S1, normalized to the number of rings on the surface. As expected, the more complex the structure (Flower>Tortoise>Butterfly>Stone-Wales), the less likely it is to be found on the surface. Nevertheless, despite the low population, the computationally inexpensive nature of the methodology described in this paper allows running enough simulated experiments to obtain relevant statistics of such structures.

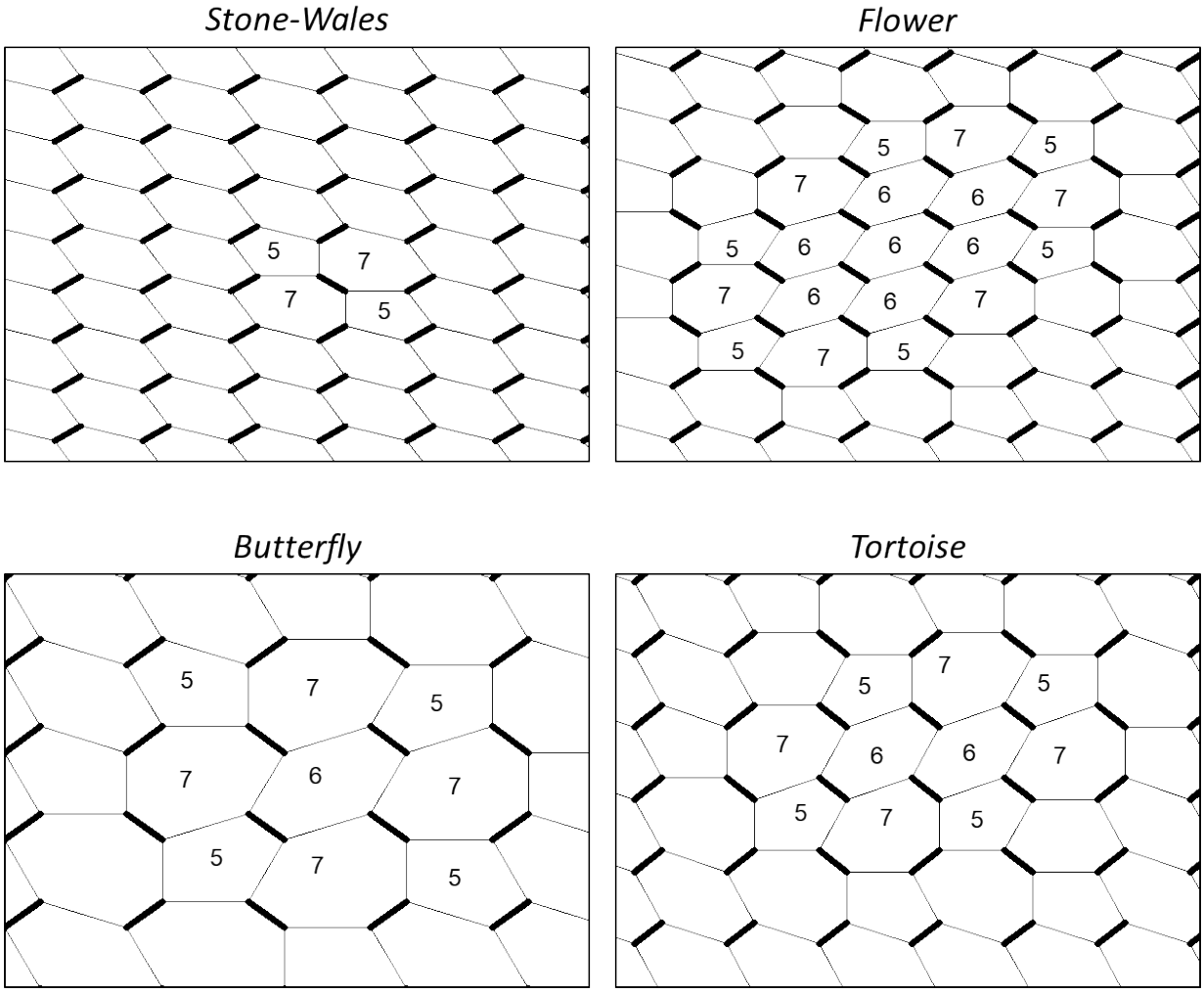

Figure 6: Different known structures obtained by successive linkage rotations.

The simplicity of the model allows it to be easily executed as a simulation using a Monte Carlo approach. To implement the simulation, a two-dimensional square lattice of $L \times L$ sites with periodic boundary conditions is considered.

The probability P of an event occurring is proportional to the Boltzmann function, and can be written as,

$$P \propto \exp\left(-\frac{\Delta E}{k_B T}\right), \tag{3}$$

where ΔE, is the difference in energy between the final and initial states, k_B is the Boltzmann´s constant, and T is the absolute temperature. The energy change associated with the linkage rotation is calculated from Eq. (2). Note that here, we have chosen a simple expression to illustrate our approach. However, reality is likely more complex, and one could write an expression for the energy dependence where longer range interactions not currently addressed, for example, could be considered. Another consideration that is not explicitly considered in the model is the impact of the support and its interaction with the bilayer. As previously mentioned, bilayer silica in Pt(111) for example does not yield crystalline structures at all, as a result of the crystalline bilayer being too far out of registry with respect to the unit cell of the Pt(111) surface .[10] This factor could be thought as inherently included in the in the energy factor ε, as the energy change associated with a bond switch event will depend on the support. Another example of such support effects was recently reported by the Altman group, where the lattice unit cell of the metal support is tuned.[39]

The Monte Carlo simulation is carried out from a given arbitrary initial configuration. The calculated probability P of an event to occur is then compared with a random number *R* distributed uniformly in $[0,1]$. If the probability P is greater than the random number *R*, the selected linkage is rotated. If it is not, the linkage remains in their original orientation. This process is repeated until the general ring size distribution does not change.

This procedure is made over 10^6 different samples for a given value of temperature, to provide statistically relevant results. The simulation uses the Kawasaki algorithm [40] for the lattice-gas model to represent a perfectly flat surface where the linkages are distributed.

The main advantage of the model is its easy implementation for Monte Carlo simulations, and different observables can be obtained quickly and efficiently.

3. Results and Discussion

3.1. Temperature dependence

The evolution of the equilibrium ring size distribution as a function of the temperature is shown in Figure 7, starting from a perfectly hexagonal structure. The simulations were performed over 10^6 different samples in lattices of size $L = 120$ with periodic boundary conditions. We define a Monte Carlo step (MCS) as a number of attempts of rotation equal to the number of cells in the lattice. For example, in the case in figure 7, with *L* = 120, 1 MCS equals 120 × 120 = 14,400 attempts of rotation. In the simulations in figure 7, it was determined that 10^6 MCS was sufficient to reach equilibrium in the ring size distribution. The statistics were calculated using an additional 10^6 MCS after equilibrium conditions were reached for each of the simulated samples. For

simplicity, we define the relative temperature (proportional to absolute temperature T), $T_r = k_B T/\varepsilon$. This relative temperature T_r can be correlated to the actual temperature if the energy parameter ε is known. Note that this is the same ε used in equation 2. for rotating a linkage is known. Given that there is literature data from density functional calculations on the energies required to produce Stone-Wales defects in silica bilayers, we can use these results to estimate the magnitude of the parameter ε. The table below provides ε values indirectly obtained from defect formation energies reported in the literature. For example, in order to form a Stone-Wales defect, from equation 2, we obtain $\Delta E = 4\varepsilon$.

Reference	Number of Stone-Wales Defects used for energy calculation	$\Delta E = 4\varepsilon\ (eV)$	$\varepsilon\ (eV)$
[25]	1	2.80	0.70
[1]	1	1.83	0.46
[1]	2	1.29	0.32
[1]	3	0.97	0.24

Table 1: Formation energy values for Stone-Wales defect obtained from literature.

As seen in table 1, there is significant variation in the obtained values of ε, even using calculations from the same reference when Stone-Wales defects have different configurations around them. This indicates that there are longer range effects than the ones we are considering in this work, or that strain induced by the periodic boundary conditions used in the relatively small unit cells achievable by ab-initio methods. Nevertheless, with this caveat in mind, we acknowledge that a more realistic representation of real systems will require careful consideration of the energy expression used. We will see in subsequent paragraphs that, despite the simplicity of our expression, the simulated experiments presented here can still capture to a reasonable extent the results from experimental data.

Going back to the results presented in Figure 7, we can see that, at T_r < 0.3, only hexagons (6-member rings) are obtained. However, as the temperature increases, a distribution of rings sizes is produced, reaching an asymptote with a fraction of hexagonal rings of ~ 0.375. This is the result of reaching a random distribution of RLs in the lattice at these high thermal energies. The asymptote fraction obtained is expected, as from the 16 possible configurations described in Figure 5, only six are hexagons (6/16 = 0.375).

Given the symmetry in the proposed model, in average, the number of squares (4-member rings) is the same as the number of octagons (8-member rings), reaching an asymptotic fraction of 0.0625 at high temperature (1/16=0.0625). In the same way, the number of pentagons (5-member rings) is the same as the number of heptagons (7-member rings), reaching a high-temperature asymptotic fraction of 0.25.

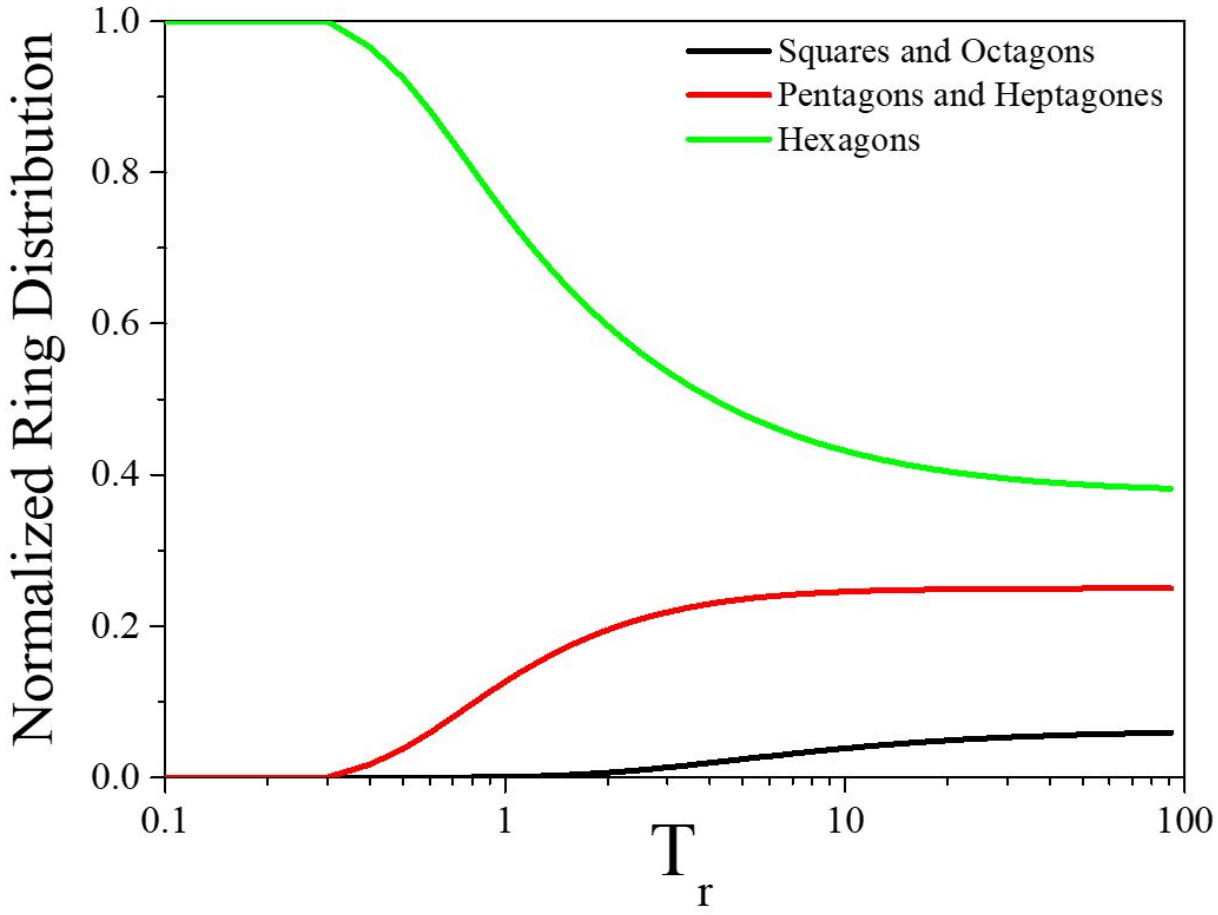

Figure 7: Evolution of the ring size distribution as function of relative temperature ($\boldsymbol{T_r = k_B T/\varepsilon}$).

Considering the distribution in Figure 7, one can compare to experimental data and find at what T_r, the simulation matches the ring size distribution in experimental results. This comparison is shown in figure 8 as histograms, where the experimental data (red bars) was taken from reference[41] by K. M. Burson et al. The averaged data from Monte Carlo simulations is shown as green bars. For the more "crystalline case" the best match corresponds to $T_r = 0.7$ (Fig. 8a) and for the vitreous case, the best match is at $T_r = 21$ (Fig. 8b). For $T_r = 0.7$, the agreement between histograms is rather good within the statistical error. At higher relative temperature ($T_r = 21$) there are differences between the experimental and simulation results are larger.

To provide an idea of variations from sample to sample, we have also included the ring size statistics for a snapshot of single simulated sample after 2×10^6 Monte Carlo Steps, and this is shown as blue bars in Fig. 8b. This "snapshot" in the simulation is similar to the case the

experimental data, were a single sample is considered, and some variation is expected with respect to the statistical distribution that one would obtain if it was practical to scan as many experimental samples as one can simulate. This illustrates the importance of considering a statistically relevant number of datapoints. While we recognize that doing this experimentally is impossible, we want to make the point that one should be cautios about it when deriving statitstics from one or a handful of images. That said, considering the data that is available in literature, there does seem to be a tendency to favor 5-member over 7-member rings in experimental systems. This assymetry is not captured by the symmetric energy relation we have chosen to use (equation 2) to introduce our approach, but this can be easily modified in the future to refine the model including energetic parameters in the equation that can be related to inherent physics and chemistry of the experimental system that may give rise to this asymetry in the distribution.

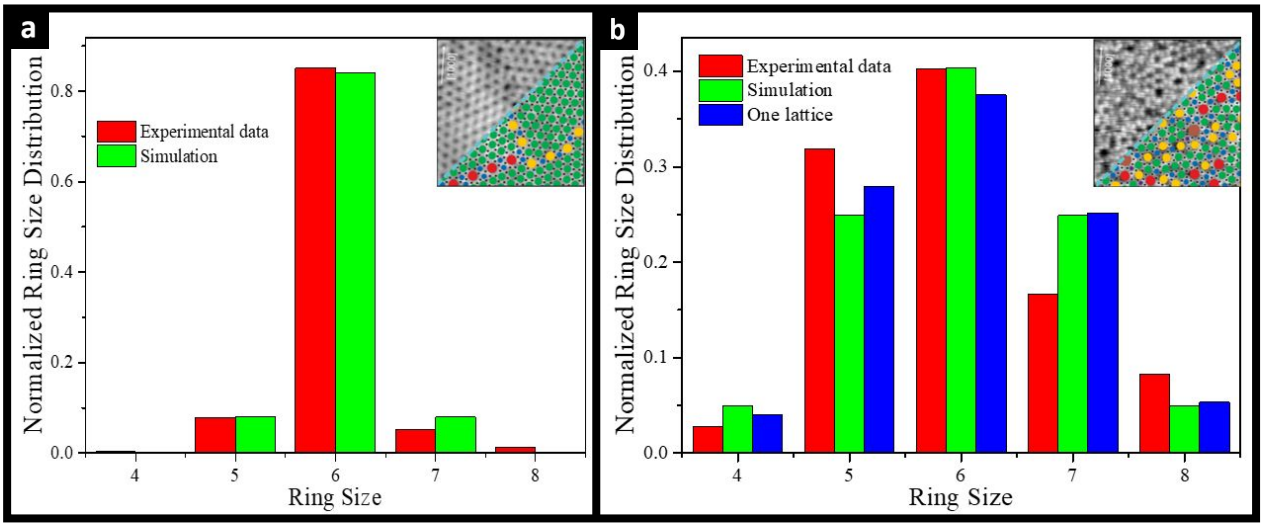

Figure 8: Ring distribution histogram, comparison between experimental data from literature and the proposed model. (a) Low ($\boldsymbol{T_r = 0.7}$) and (b) high ($\boldsymbol{T_r = 21}$) relative temperatures. Inset STM images reproduced from [[41]].

Snapshots of the simulated system at $T_r = 0.7$ and $T_r = 21$ are shown in Figures 9a and 9b, respectively. To aid in the visualization of the ring arrangements, we have color-coded them such that hexagons are shown in red, pentagons in blue, heptagons in green, squares in purple, and octagons with a black dot in the center. Portions of the system where the rings have been relaxed are shown in Figures 9c and 9d respectively. From a visual inspection of Figure 9a, one can identify another difference with the experimental system. This relates to the formation of chains of

alternating ring sizes experimentally, resulting in domain boundaries. These are likely related to a longer-range effect (possibly strain) and thus also not captured in the simple version of the energy relation used in the model where only first neighbors affect the probability of a linkage rotation to take place. Experimental and theoretical work has shown that strain does play an important role in the ring size distribution, and the formation of defect lines.[38] [39]

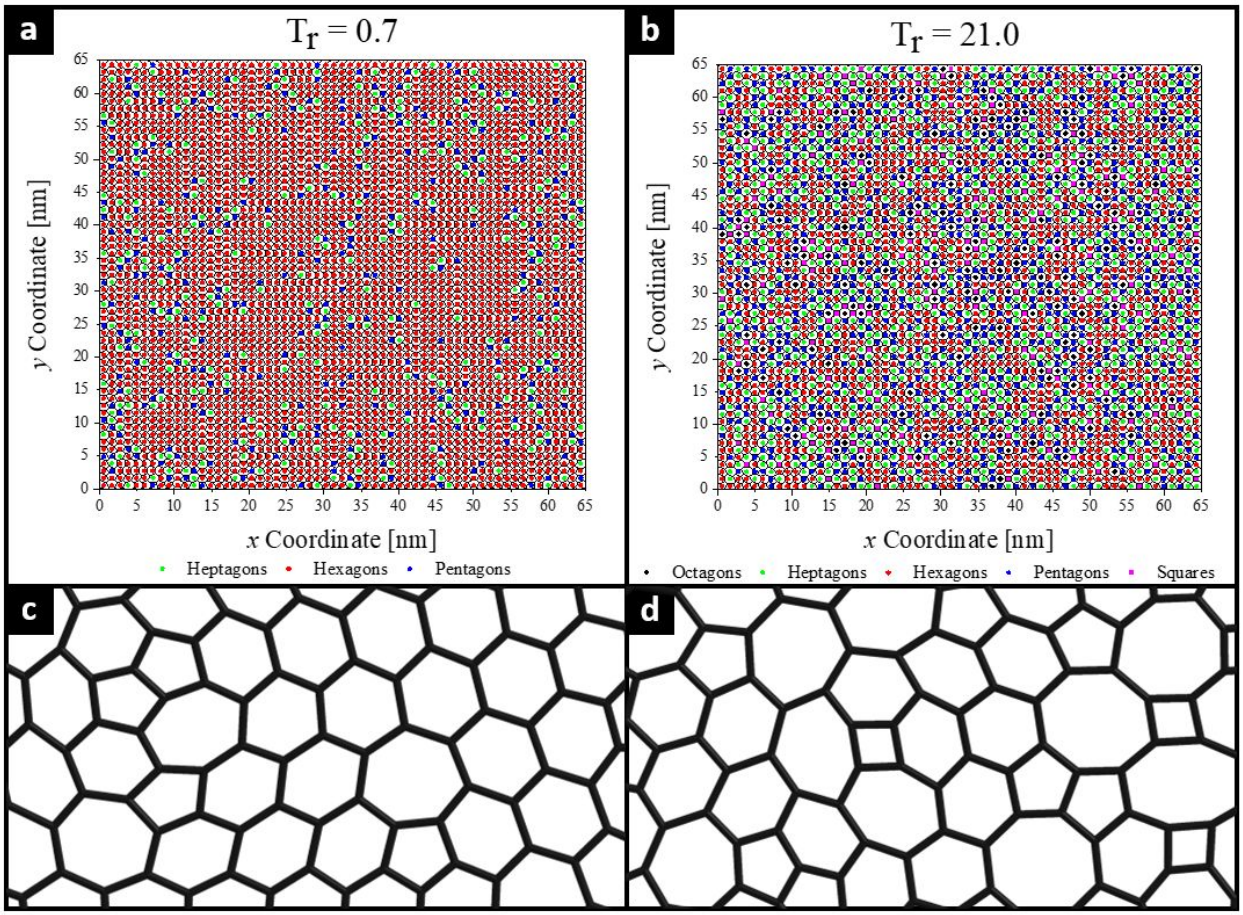

Figure 9: Structural representation and a portion of relaxed of the system at (a and c) low and (b and d) high relative temperature.

From atomically resolved STM image of a crystalline–vitreous boundary in a bilayer silica film Lichtenstein et al [9], obtained a plot showing how the distribution of ring sizes changes when going through such transition, which takes place within just a few nanometers. It is remarkable that such transition can take place within a small space. A likely scenario to reach this is that a local perturbation may be present in the system during the synthesis to achieve such distribution. With our model, a comparable ring size distribution can be obtained by setting a temperature gradient through the system at this timescale. In figure 10, we show the experimental ring size

distribution obtained by Lichtenstein et al overlaid with that from simulated experiments. The left end of the slab in the simulated experiment is set to a low temperature, while the right end is set to a high temperature. The gradient is shown graphically in Figure 10a with a T_r going from 0.1 to 25. Monte Carlo simulations on lattices of different sizes (L = 48, 60, and 120) are performed for comparison. Each lattice has periodic boundary conditions only in the vertical direction. 10^6 simulated experiments are considered to obtain the shown statistics. The results slightly depend on the lattice size, and they show a good agreement with the experiment data to reproduce the distribution of the rings in the system. Note that we do not imply by any means that such large gradients exist in the experiment during synthesis of the material. While temperature gradients may be present in the sample, these should not be nearly as large as those needed in the simulation to reach this distribution and they span larger distances. Using a temperature gradient in the simulation could however be used as a proxy in this simple model as a proxy for other type of short-range perturbations that may be giving rise to the formation of this domain. Future versions of the simulated model could include for example more explicit energy relations associated with local perturbations in the system to account for these experimental findings.

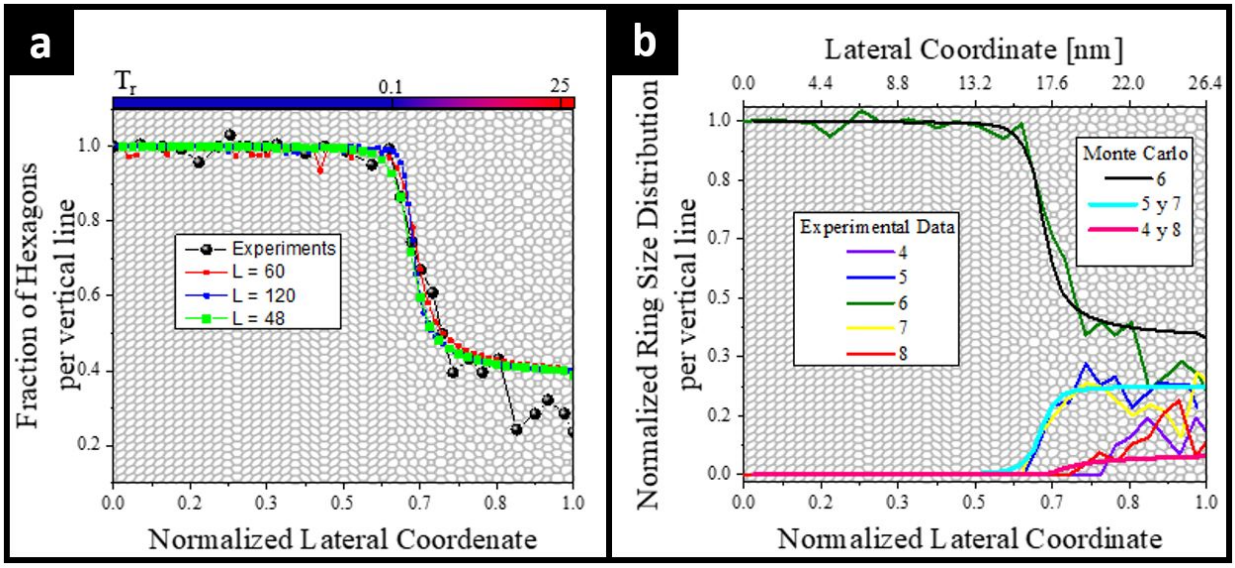

Figura 10: a) Relative amount of hexagons as a function of normalized lateral coordinate for different lattice sizes, relative temperature gradient is show in the upper part. b) relative amount of the rings vs lateral coordinate for both experimental data and Monte Carlo, with the same relative temperature gradient as used in a).

3.2. Dynamics.

Another advantage of this simple model is the possibility of investigating the dynamics of the system during its simulated synthesis. To illustrate this, we follow the temporal evolution (where time is in Monte Carlo steps) for systems starting from an ordered array of Stone-Wales defects (Fig. 11a) and from a random distribution of ring sizes (Fig. 11b) at a low relative temperature ($T_r = 0.1$). While both systems tend to the perfectly hexagonal configuration as the time passes, there are is an important difference which is evident when paying close attention to the distribution of pentagons and heptagons at long MC times. For the case starting from Stone-Wales defects, the thermodynamically most stable configuration of the hexagonal lattice is reached faster. However, for the random starting distribution in Fig. 11b, at the longer time scales, there is still a sizable population of heptagons and pentagons. This related to the fact that pentagons and heptagons tend to stay isolated from each other at low concentrations in the random system, and the probability of finding a configuration of two 5-member rings and two 7-member rings arranged spatially in a way that can result in an inverse SW movement to convert them to four 6-member rings is very low. At infinite times, the values shown in Figure 7 are expected to be recovered.

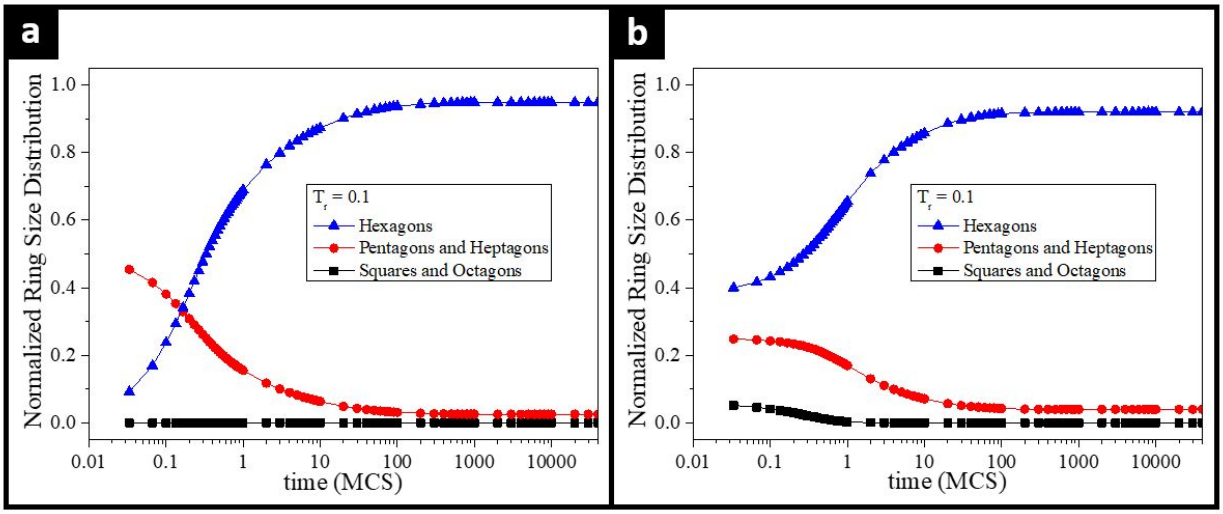

Figure 11: Dynamic evolution of (a) a complete Stone-Wales array and (b) completely random array at low relative temperature.

4. Summary and Conclusions

In this work we have presented a simple and computationally inexpensive method to represent two-dimensional bilayer silicates as a network of rings that can transform by rotating their edges. The model uses a Monte Carlo method and a bond-switching algorithm to allow for

transformations between configurations of different ring size distributions in the system, the two extremes being a perfectly crystalline hexagonal system and one with a random distribution of ring sizes. Such configurations have been previously observed experimentally but the conditions that lead to specific ring arrangements and how transformations occur between them are not clearly understood. Through the work, we compare the results of the experimental systems and the simulated experiments focusing on statistics of ring size distributions. We also showing how the proposed model can shed light into processes more challenging to study experimentally, such as the dynamics of these transformations and formation of boundaries between different configurations.

The probability of rotating edges of the rings to lead to new configurations is a function of the change in energy associated with this rotation, and the temperature of the system. In the simulations described in this work, we have chosen a very simple and symmetric geometrical energy relation to calculate the probably of each event attempted. While this relation captures some of the behavior of the experimental system, and illustrates the strength and simplicity of the model (which is the main purpose of this manuscript), a more complex and realistic energy relation that also accounts to longer ranger effects will be needed to more holistically capture the underlaying chemistry and physics associated with these transformations. This simple method, in concert with experimental data, and more computationally expensive methods to obtain specific energy parameters for the system, can aid in reaching a better understanding of the formation of crystalline versus glassy silicates and the transformations between them.

References

[1] L. Lichtenstein *et al.*, “The atomic structure of a metal-supported vitreous thin silica film,” *Angew. Chemie - Int. Ed.*, vol. 51, no. 2, pp. 404–407, 2012.

[2] P. Y. Huang *et al.*, “Direct imaging of a two-dimensional silica glass on graphene,” *Nano Lett.*, vol. 12, no. 2, pp. 1081–1086, 2012.

[3] W. H. Zachariasen, “The atomic arrangement in glass,” *J. Am. Chem. Soc.*, vol. 54, no. 10, pp. 3841–3851, 1932.

[4] C. Büchner *et al.*, “Ultrathin silica films: The atomic structure of two-dimensional crystals and glasses,” *Chem. - A Eur. J.*, vol. 20, no. 30, 2014.

[5] D. Loffler *et al.*, “Growth and Structure of Crystalline Silica Sheet on Ru(0001),” *Phys. Rev. Lett.*, vol. 105, no. 14, p. 4, 2010.

[6] H. J. Kreuzer and J. Zhang, “Kinetic lattice gas-model: Langmuir, Ising and interaction kinetics,” *Appl. Phys. a-Materials Sci. Process.*, vol. 51, no. 3, pp. 183–190, 1990.

[7] H. W. Klemm *et al.*, “Formation and Evolution of Ultrathin Silica Polymorphs on Ru(0001) Studied with Combined in Situ, Real-Time Methods,” *J. Phys. Chem. C*, vol. 123, no. 13, pp. 8228–8243, Apr. 2019.

[8] H. W. Klemm *et al.*, “A Silica Bilayer Supported on Ru(0001): Following the Crystalline-to Vitreous Transformation in Real Time with Spectro-microscopy,” *Angew. Chemie - Int. Ed.*, vol. 59, no. 26, pp. 10587–10593, Jun. 2020.
[9] L. Lichtenstein, M. Heyde, and H. J. Freund, “Crystalline-vitreous interface in two dimensional silica,” *Phys. Rev. Lett.*, vol. 109, no. 10, p. 106101, 2012.
[10] X. Yu, B. Yang, J. A. Boscoboinik, S. Shaikhutdinov, and H. J. Freund, “Support effects on the atomic structure of ultrathin silica films on metals,” *Appl. Phys. Lett.*, vol. 100, no. 15, p. 151608, 2012.
[11] B. Yang *et al.*, “Thin silica films on Ru(0001): Monolayer, bilayer and three-dimensional networks of [SiO 4] tetrahedra,” *Phys. Chem. Chem. Phys.*, vol. 14, no. 32, pp. 11344–11351, 2012.
[12] E. Groppo, C. Lamberti, S. Bordiga, G. Spoto, and A. Zecchina, “The structure of active centers and the Ethylene Polymerization mechanism on the Cr/SiO2 catalyst: A frontier for the characterization methods,” *Chem. Rev.*, vol. 105, no. 1, pp. 115–183, 2005.
[13] J. A. Boscoboinik *et al.*, “Modeling zeolites with metal-supported two-dimensional aluminosilicate films,” *Angew. Chemie - Int. Ed.*, vol. 51, no. 24, pp. 6005–6008, 2012.
[14] J. A. Boscoboinik, X. Yu, B. Yang, S. Shaikhutdinov, and H. J. Freund, “Building blocks of zeolites on an aluminosilicate ultra-thin film,” *Microporous Mesoporous Mater.*, vol. 165, pp. 158–162, 2013.
[15] W. Loewenstein, “The distribution of aluminum in the tetrahedra of silicates and aluminates.,” *Am. Mineral.*, vol. 39, p. 92, 1954.
[16] J. A. Boscoboinik, “Chemistry in confined space through the eyes of surface science - 2D porous materials,” *J. Phys. Condens. Matter*, vol. 31, no. 6, 2019.
[17] M. Wang *et al.*, “Mechanism of the Accelerated Water Formation Reaction under Interfacial Confinement,” *ACS Catal.*, vol. 10, no. 11, pp. 6119–6128, Jun. 2020.
[18] M. J. Prieto *et al.*, “Water Formation under Silica Thin Films: Real-Time Observation of a Chemical Reaction in a Physically Confined Space,” *Angew. Chemie Int. Ed.*, vol. 57, no. 28, pp. 8749–8753, 2018.
[19] J.-Q. Zhong, M. Wang, N. Akter, D. Stacchiola, D. Lu, and J. Boscoboinik, “Room-Temperature in Vacuo Chemisorption of Xenon Atoms on Ru(0001) under Interface Confinement,” *J. Phys. Chem. C*, vol. 123, no. 22, pp. 13578–13585.
[20] B. Yao, S. Mandrà, J. O. Curry, S. Shaikhutdinov, H.-J. Freund, and J. Schrier, “Gas Separation through Bilayer Silica, the Thinnest Possible Silica Membrane,” *ACS Appl. Mater. Interfaces*, vol. 9, no. 49, pp. 43061–43071, Dec. 2017.
[21] N. Metropolis, A. W. Rosenbluth, M. N. Rosenbluth, A. H. Teller, and E. Teller, “Equation of state calculations by fast computing machines,” *J. Chem. Phys.*, vol. 21, no. 6, pp. 1087–1092, 1953.
[22] D. P. Landau and K. Binder, *A Guide to Monte Carlo Simulations in Statistical Physics*. 2009.
[23] F. Wooten, K. Winer, and D. Weaire, “Computer generation of structural models of amorphous Si and Ge,” *Phys. Rev. Lett.*, vol. 54, no. 13, pp. 1392–1395, 1985.
[24] F. Wooten and D. Weaire, “Modeling Tetrahedrally Bonded Random Networks by Computer,” *Solid State Phys. - Adv. Res. Appl.*, vol. 40, no. C, pp. 1–32, 1987.
[25] G. Barkema and N. Mousseau, “High-quality continuous random networks,” *Phys.*

Rev. B - Condens. Matter Mater. Phys., vol. 62, no. 8, pp. 4985–4990, 2000.
[26] R. L. C. Vink and G. T. Barkema, “Large well-relaxed models of vitreous silica, coordination numbers, and entropy,” *Phys. Rev. B - Condens. Matter Mater. Phys.*, vol. 67, no. 24, p. 245201, 2003.
[27] R. L. C. Vink, G. T. Barkema, M. A. Stijnman, and R. H. Bisseling, “Device-size atomistic models of amorphous silicon,” *Phys. Rev. B - Condens. Matter Mater. Phys.*, vol. 64, no. 24, pp. 2452141–2452146, 2001.
[28] A. Nakano, R. K. Kalia, and P. Vashishta, “First sharp diffraction peak and intermediate-range order in amorphous silica: finite-size effects in molecular dynamics simulations,” *J. Non. Cryst. Solids*, vol. 171, no. 2, pp. 157–163, 1994.
[29] E. I. Benegas, V. D. Pereyra, and G. Zgrablich, “On the behaviour of adsorption isotherms of a Lennard-Jones gas on a disordered lattice,” *Surf. Sci. Lett.*, vol. 187, no. 1, pp. L647–L653, 1987.
[30] J. Kotakoski, A. V. Krasheninnikov, U. Kaiser, and J. C. Meyer, “From point defects in graphene to two-dimensional amorphous carbon,” *Phys. Rev. Lett.*, vol. 106, no. 10, p. 105505, 2011.
[31] A. Kumar, M. Wilson, and M. F. Thorpe, “Amorphous graphene: A realization of Zachariasens glass,” *J. Phys. Condens. Matter*, vol. 24, no. 48, p. 485003, 2012.
[32] T. Aste and D. Sherrington, “Glass transition in self-organizing cellular patterns,” *J. Phys. A. Math. Gen.*, vol. 32, no. 41, pp. 7049–7056, 1999.
[33] P. K. Roy, M. Heyde, and A. Heuer, “Modelling the atomic arrangement of amorphous 2D silica: A network analysis,” *Phys. Chem. Chem. Phys.*, vol. 20, no. 21, pp. 14725–14739, 2018.
[34] P. K. Roy and A. Heuer, “Relating local structures, energies, and occurrence probabilities in a two-dimensional silica network,” *J. Phys. Condens. Matter*, vol. 31, no. 22, 2019.
[35] P. K. Roy and A. Heuer, “Ring Statistics in 2D Silica: Effective Temperatures in Equilibrium,” *Phys. Rev. Lett.*, vol. 122, no. 1, 2019.
[36] P. N. Keating, “Effect of invariance requirements on the elastic strain energy of crystals with application to the diamond structure,” *Phys. Rev.*, vol. 145, no. 2, pp. 637–645, 1966.
[37] J. Tersoff, “New empirical approach for the structure and energy of covalent systems,” *Phys. Rev. B*, vol. 37, no. 12, pp. 6991–7000, 1988.
[38] T. Björkman *et al.*, “Defects in bilayer silica and graphene: Common trends in diverse hexagonal two-dimensional systems,” *Sci. Rep.*, vol. 3, no. 1, p. 3482, 2013.
[39] C. Zhou *et al.*, “Tuning two-dimensional phase formation through epitaxial strain and growth conditions: silica and silicate on NixPd1−x(111) alloy substrates,” *Nanoscale*, vol. 11, no. 44, pp. 21340–21353, 2019.
[40] K. Kawasaki, “Diffusion constants near the critical point for time-dependent ising models. I,” *Phys. Rev.*, vol. 145, no. 1, pp. 224–230, 1966.
[41] K. M. Burson, C. Büchner, M. Heyde, and H. J. Freund, “Assessing the amorphousness and periodicity of common domain boundaries in silica bilayers on Ru(0 0 0 1),” *J. Phys. Condens. Matter*, vol. 29, no. 3, p. 035002, 2017.

Ring size distribution in silicate bilayers obtained from Monte Carlo simulations using a bond-switching algorithm (compared to experimental data) when a temperature gradient is introduced to mimic a crystalline to vitreous domain boundary.

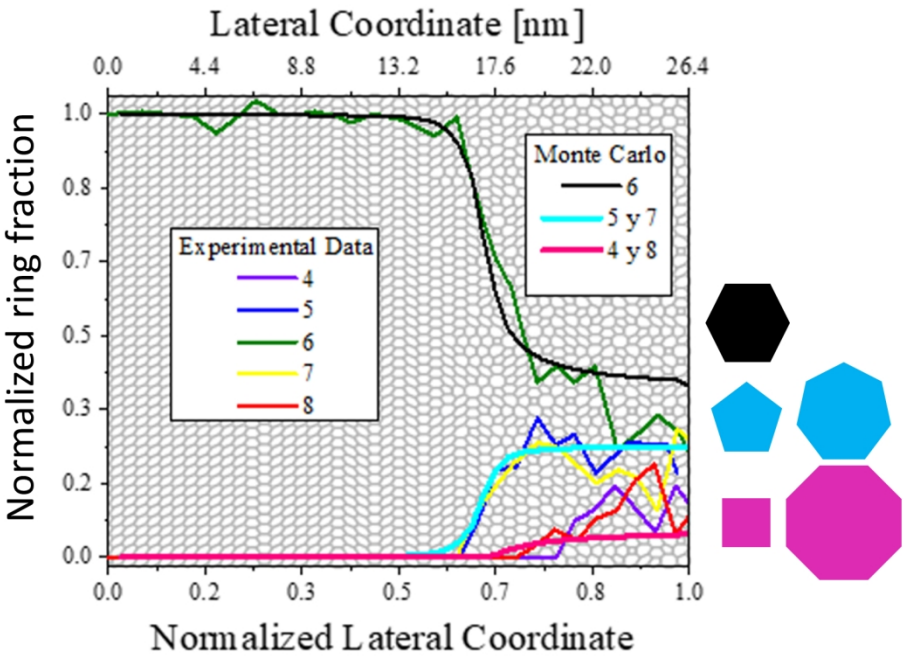
Lateral Coordinate [nm]
0.0
4.4
8.8
13.2
17.6
22.0
26.4
Normalized ring fraction
1.0
0.8
0.7
0.5
0.3
0.2
0.0
Experimental Data
4
5
6
7
8
Monte Carlo
6
5 y 7
4 y 8
0.0
0.2
0.3
0.5
0.7
0.8
1.0
Normalized Lateral Coordinate